Reconciling the Observed and Modeled Southern Hemisphere Circulation Response to Volcanic Eruptions–Supplemental Material

Marie C. McGraw[1], Elizabeth A. Barnes[1], and Clara Deser[2]

Contents:

Corresponding author: Marie C. McGraw (mmcgraw@atmos.colostate.edu)

[1]Department of Atmospheric Science,

Colorado State University, Fort Collins,

Colorado, USA.

[2]Climate and Global Dynamics Division,

National Center for Atmospheric Research,

Boulder, Colorado, USA.

1. Selection of CMIP5 Models (Figure S1 and Table S1)

Not all of the CMIP5 'historical' forcing simulations include volcanic forcing. Following previous studies (e.g. *Santer et al.* [2013]), we use a lower stratospheric temperature anomaly (TLS) to determine whether or not a model demonstrates a strong enough response to volcanic forcing. Similar to *Santer et al.* [2013], we define the TLS as the zonal mean temperature anomaly at 50 hPa from 82.5°S-82.5°N. For each model, the ensemble mean TLS must exceed 0.5°C in at least one of the twelve months following the El Chichón and Pinatubo eruptions for the to be included in our analysis. The mean TLS of the models that did exhibit a sufficient forced response, as well as the TLS of the models that were excluded, can be seen in Figure S1. This selection process is not sensitive to where we set the threshold; the same models were excluded if the threshold temperature was set at 0.25°C or at 0.75°C.

Figure S1 demonstrates that the 9 models that were excluded–the three CMCC models (CMCC-CM, CMCC-CMS, CMCC-CESM), FGOALS-g2, FIO-ESM, the three IPSL models (IPSL-CM5B-LR, IPSL-CM5A-MR, IPSL-CM5A-LR), and inmcm4–lack the clear lower stratospheric temperature increase that is a hallmark of volcanic forcing. Other studies (e.g. *Santer et al.* [2013], *Lehner et al.* [2016]) exclude the same models for similar reasons. Ultimately, a total of 37 models and 155 simulations are used in the CMIP5 analysis; a full list of these models and simulations is given in Table S1.

2. Midlatitude Jet Results (Figure S2)

In addition to analyzing changes in the circulation using the Southern Annular Mode (SAM), we also analyze changes in the midlatitude jet explicitly by calculating changes in

the 10-meter zonal mean zonal winds. An advantage of using the 10-meter zonal winds is that changes in these winds can be directly connected to changes in ocean surface stress, thus linking atmospheric to potential oceanic changes. The results at 700 hPa and 10-m are similar (not shown). The Southern Hemisphere midlatitude jet is calculated using the zonal wind anomalies at all longitudes between 20-80°S, from 1970-2004 (1979-2004 for the MERRA reanalysis data). The jet position is defined by identifying the maximum of the zonal-mean zonal wind at the level of interest (in this case, 10 meters above the surface), and then fitting a second-order polynomial through the wind maximum. The midlatitude jet position and strength are defined as the location and the magnitude of the maximum of this polynomial. 10-meter zonal winds were not available for the CESM-Pacemaker simulations, so only the CESM1 Large Ensemble (CESM-LE) and MERRA reanalysis were analyzed.

Figure S2 shows the histogram of anomalous NDJ jet position (Figure S2a) and jet strength (Figure S2b). Years following El Chichón (1982-1983) and Pinatubo (1991-1992) are in red, while all other years are in blue; the observed responses to El Chichón (dashed line) and Pinatubo (solid line) are shown in black. The eddy-driven jet results present a similar picture to the SAM results (Figure 2), showing a poleward shift and a strengthening of the 10-m zonal winds following eruptions. In both cases, the internal variability remains considerable, with equatorward shifts and weakening of the 10-meter zonal mean zonal winds occurring after volcanoes in some simulations. The distributions for years following eruptions and for all other years for both jet position and jet strength are significantly different at 95% confidence using a two-sample K-S test. As with the SAM indices, the MERRA reanalysis results fall within the range of internal variability,

indicating that, while the forced response to a volcanic eruption is that of a positive SAM/poleward shift/strengthening of the eddy-driven jet, internal variability is great enough that a negative SAM/equatorward shift/weakening of the eddy-driven jet can all occur following a volcanic eruption.

The relationship between the eddy-driven jet and the state of the El Niño-Southern Oscillation (ENSO) is less clear than the relationship between the SAM and ENSO (see Figure 4 and discussion). While the eddy-driven jet shifts poleward and strengthens regardless of ENSO state, these changes are generally not significant, and do not exhibit a clear relationship with ENSO state (not shown). The eddy-driven jet is inherently more variable than the SAM–the eddy-driven jet is a maximum, while the SAM is a large-scale pattern calculated over 60°of latitude. Therefore, while the eddy-driven jet results support the conclusions drawn using the SAM, the effect of ENSO state on the eddy-driven jet response to volcanoes is not as clear.

3. Combined CMIP5-CESM1 Results for ENSO State Analysis (Figure S3)

In addition to analyzing the CESM1 and CMIP5 results separately, we also combined all simulations from CESM1 and CMIP5 and analyzed the relationship between the ENSO state and the volcanically-forced SAM response. By combining the CESM1 and CMIP5 runs, we are able to analyze over 200 simulations across 2 eruptions, thereby giving us over 400 volcanically-influenced circulation anomalies. Figure S3 shows the results of the combined analysis. A significant forced positive SAM is seen following a volcanic eruption for all three ENSO states, and is significant at 95% confidence using a one-sided signed rank test. Additionally, the volcanically-forced SAM response during negative ENSO events is significantly more positive than the SAM response following negative

ENSO events, with this significance improved to the 95% confidence level (again, using a one-sided signed rank test).

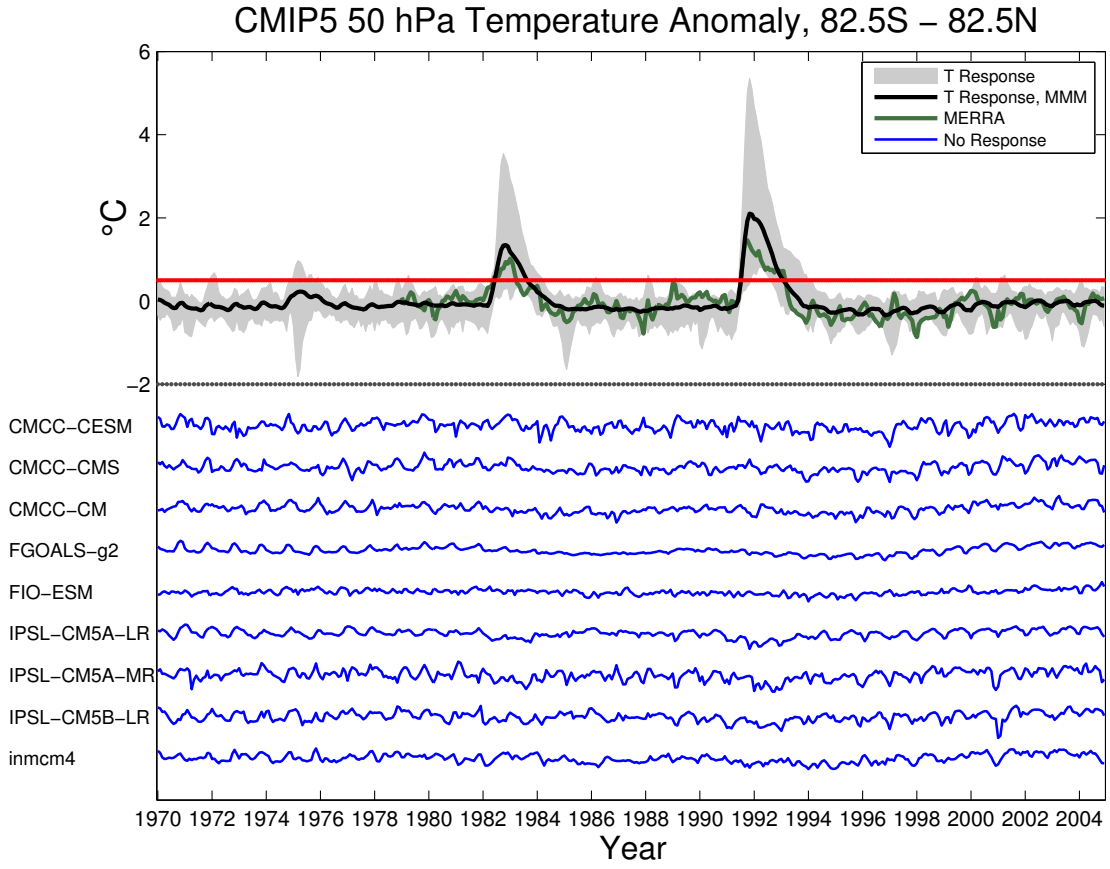

Figure 1. 50 hPa zonal mean temperature anomalies for the CMIP5 models. The gray shading indicates the range of temperature anomalies across the 37 CMIP5 models that demonstrated a strong enough temperature response to volcanic forcing (at least 0.5°C, denoted by the red line), and the black line is the multi-model mean of these 37 models. The observed changes in 50 hPa zonal mean temperature anomalies are shown in green. The 9 models that did not exhibit an adequate 50 hPa temperature response are shown in blue.

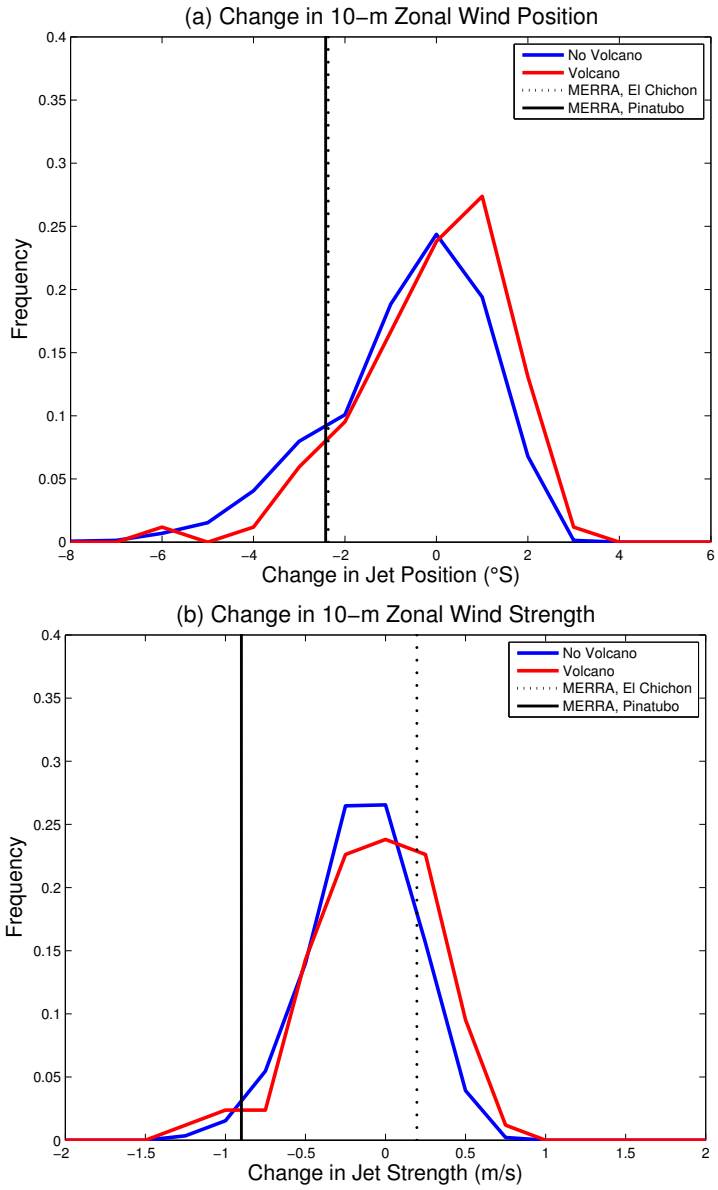

Figure 2. The distribution of NDJ changes in near-surface (10 meter) (a) jet position and (b) jet strength for years without volcanoes (blue lines) and years with volcanoes (red lines) for the CESM-LE. The observed changes in jet position and strength following El Chichón (dashed lines) and Pinatubo (solid lines) are in black.

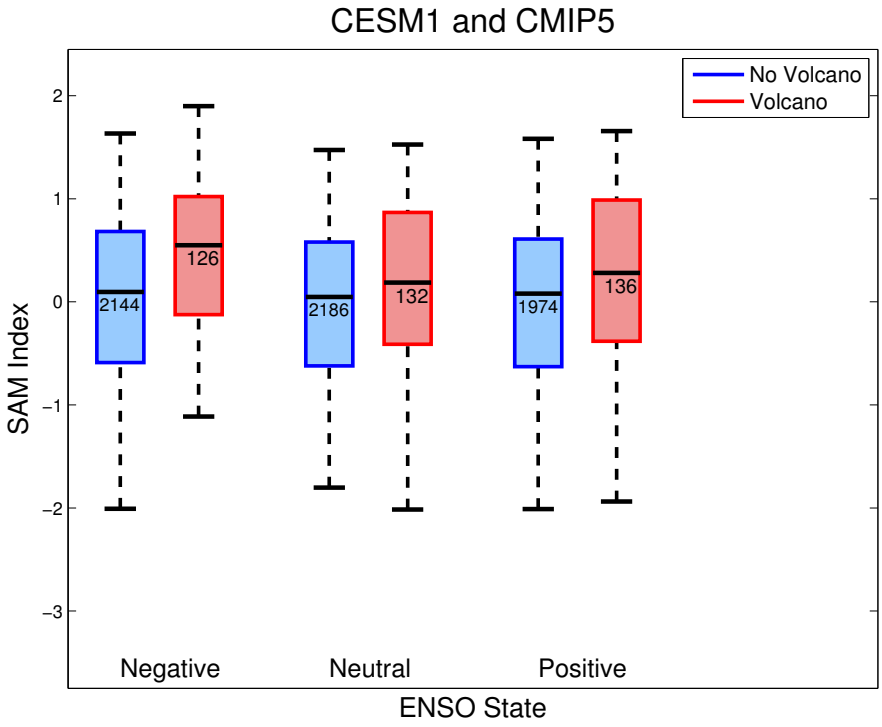

Figure 3. Mean NDJ SAM index as a function of ENSO state for all CESM-LE and CMIP5 simulations. Years following volcanoes are in red, while all other years are in blue. Shaded boxes indicate that the median value of the SAM index in years with volcanoes is significantly different from that in years without volcanoes at 95% confidence. The numbers inside the boxes list the number of simulations in each ENSO state. The whiskers show the 95th percentile range across the simulations.

Table 1. CMIP5 'historical' simulations used to calculate the circulation response to volcanic forcing.

Model	Ensemble Member
ACCESS 1-0	r1i1p1
ACCESS 1-3	r1i1p1
bcc-csm1-1	r1i1p1
bcc-csm1-1	r2i1p1
bcc-csm1-1	r3i1p1
bcc-csm1-1-m	r1i1p1
bcc-csm1-1-m	r2i1p1
bcc-csm1-1-m	r3i1p1
BNU-ESM	r1i1p1
CanCM4	r1i1p1
CanCM4	r2i1p1
CanCM4	r3i1p1
CanCM4	r4i1p1
CanCM4	r5i1p1
CanCM4	r6i1p1
CanCM4	r7i1p1
CanCM4	r8i1p1
CanCM4	r9i1p1
CanCM4	r10i1p1
CanESM2	r1i1p1
CanESM2	r2i1p1
CanESM2	r3i1p1
CanESM2	r4i1p1
CanESM2	r5i1p1
CCSM4	r1i1p1
CCSM4	r2i1p1
CCSM4	r3i1p1
CCSM4	r4i1p1
CCSM4	r5i1p1
CCSM4	r6i1p1
CESM1-BCG	r1i1p1
CESM1-CAM5	r1i1p1
CESM1-CAM5	r2i1p1
CESM1-CAM5	r3i1p1
CESM1-CAM5-1-FV2	r1i1p1
CESM1-CAM5-1-FV2	r2i1p1
CESM1-CAM5-1-FV2	r3i1p1
CESM1-CAM5-1-FV2	r4i1p1
CESM1-FASTCHEM	r1i1p1
CESM1-FASTCHEM	r2i1p1
CESM1-FASTCHEM	r3i1p1
CESM1-WACCM	r1i1p1
CESM1-WACCM	r2i1p1
CESM1-WACCM	r3i1p1
CESM1-WACCM	r4i1p1
CNRM-CM5	r1i1p1
CNRM-CM5	r2i1p1
CNRM-CM5	r3i1p1
CNRM-CM5	r4i1p1
CNRM-CM5	r5i1p1
CNRM-CM5	r6i1p1
CNRM-CM5	r7i1p1
CNRM-CM5	r8i1p1
CNRM-CM5	r9i1p1
CNRM-CM5	r10i1p1
CNRM-CM5-2	r1i1p1
CSIRO-Mk3-6-0	r1i1p1
CSIRO-Mk3-6-0	r2i1p1
CSIRO-Mk3-6-0	r3i1p1
CSIRO-Mk3-6-0	r4i1p1
CSIRO-Mk3-6-0	r5i1p1
CSIRO-Mk3-6-0	r6i1p1
CSIRO-Mk3-6-0	r7i1p1
CSIRO-Mk3-6-0	r8i1p1
CSIRO-Mk3-6-0	r9i1p1
CSIRO-Mk3-6-0	r10i1p1
FGOALS-s2	r1i1p1
FGOALS-s2	r2i1p1
FGOALS-s2	r3i1p1
GFDL-CM2p1	r1i1p1
GFDL-CM2p1	r2i1p1
GFDL-CM2p1	r3i1p1
GFDL-CM2p1	r4i1p1
GFDL-CM2p1	r5i1p1
GFDL-CM2p1	r6i1p1
GFDL-CM2p1	r7i1p1
GFDL-CM2p1	r8i1p1
GFDL-CM2p1	r9i1p1
GFDL-CM2p1	r10i1p1
GFDL-CM3	r1i1p1
GFDL-CM3	r2i1p1
GFDL-CM3	r3i1p1

Model	Ensemble Member
GFDL-CM3	r4i1p1
GFDL-CM3	r5i1p1
GFDL-ESM2G	r1i1p1
GFDL-ESM2M	r1i1p1
GISS-E2-H	r1i1p1
GISS-E2-H	r1i1p2
GISS-E2-H	r2i1p1
GISS-E2-H	r2i1p2
GISS-E2-H	r3i1p1
GISS-E2-H	r3i1p2
GISS-E2-H	r4i1p1
GISS-E2-H	r4i1p2
GISS-E2-H	r5i1p1
GISS-E2-H	r5i1p2
GISS-ED-H-CC	r1i1p1
GISS-E2-H	r1i1p1
GISS-E2-R	r1i1p2
GISS-E2-R	r1i1p3
GISS-E2-R	r2i1p1
GISS-E2-R	r2i1p2
GISS-E2-R	r2i1p3
GISS-E2-R	r3i1p1
GISS-E2-R	r3i1p2
GISS-E2-R	r3i1p3
GISS-E2-R	r4i1p1
GISS-E2-R	r4i1p2
GISS-E2-R	r4i1p3
GISS-E2-R	r5i1p1
GISS-E2-R	r5i1p2
GISS-E2-R	r5i1p3
GISS-E2-R	r6i1p1
GISS-E2-R-CC	r1i1p1
HADCM3	r1i1p1
HADCM3	r2i1p1
HADCM3	r3i1p1
HADCM3	r4i1p1
HADCM3	r5i1p1
HADCM3	r6i1p1
HADCM3	r7i1p1
HADCM3	r8i1p1
HADCM3	r9i1p1
HADCM3	r10i1p1
HadGEM2-CC	r1i1p1
HadGEM2-CC	r2i1p1
HadGEM2-CC	r3i1p1
HadGEM2-ES	r1i1p1
HadGEM2-ES	r2i1p1
HadGEM2-ES	r3i1p1
HadGEM2-ES	r4i1p1
MIROC5	r1i1p1
MIROC5	r2i1p1
MIROC5	r3i1p1
MIROC5	r4i1p1
MIROC5	r5i1p1
MIROC-ESM	r1i1p1
MIROC-ESM	r2i1p1
MIROC-ESM	r3i1p1
MIROC-ESM-CHEM	r1i1p1
MPI-ESM-LR	r1i1p1
MPI-ESM-LR	r2i1p1
MPI-ESM-LR	r3i1p1
MPI-ESM-MR	r1i1p1
MPI-ESM-MR	r2i1p1
MPI-ESM-MR	r3i1p1
MPI-ESM-P	r1i1p1
MRI-CGCM3	r1i1p1
MRI-CGCM3	r2i1p1
MRI-CGCM3	r3i1p1
MRI-CGCM3	r4i1p1
MRI-ESM1	r1i1p1
NorESM1-M	r1i1p1
NorESM1-M	r2i1p1
NorESM1-M	r3i1p1
NorESM1-ME	r1i1p1